Towards Collaborative Robots with Sensory Awareness: Preliminary Results Using Multi-Modal Sensing

Andrew L. Orekhov[1], Garrison L.H. Johnston[1], Colette Abah[1], Howie Choset[2], Nabil Simaan[1†]

***Abstract*— Current robotic systems are unable to achieve safe operation and mapping in confined spaces using intrinsic sensory data only. Recent advancement in sensory technologies in terms of miniaturization and affordability has allowed the creation of a new multi-modal sensory robot skin that can potentially achieve mapping and allow safe operation. Such robot skins may also benefit users in cases of telemanipulation, which is often hindered by limited situational awareness. In this paper, we focus on identifying the potential benefits of such robots within the context of collaborative manufacturing in confined spaces and present an experimental testing of a 4 degree-of-freedom test platform with multiple sensing disks. We demonstrate the use of the sensing skin for bracing against the environment and for avoiding collision with a human and/or the environment using proximity sensing. We also show physical human-robot interaction using Hall-effect contact sensors. We believe such robots with intrinsic distributed sensing along their entire length can enable a variety of applications in manufacturing and search and rescue domains.**

***Index Terms*— Robot perception, Collaborative robots, Continuum robots, Bracing, Mapping.**

I. Introduction

Many industrial tasks, such as aircraft maintenance and repair, require workers to exert sustained forces in unergonomic, confined postures. This type of activity can undermine the long term health of industrial workers, putting them at risk of developing conditions such as work related musculoskeletal disorders (WMSD) [1]. WMSDs are a widespread problem affecting the quality of life of industrial workers. In 2013, WMSD accounted for 33% of all injury and illness cases reported to the U.S. Bureau of Labor Statistics [2].

Automation can alleviate worker effort for simple tasks, but many cases are too complex to be completely automated. This has motivated a push to develop collaborative robots which are capable of exerting the necessary forces to complete a task while being guided by a human operator [3–5]. In scenarios where the task requires entry into a confined space, the alternative of using telemanipulated robots (*ex-situ* collaboration) seems attractive, but limitations of user situational awareness due to sensory masking render this option possible only for structured environments where exact knowledge of the constrained workspace is available to the high-level controller.

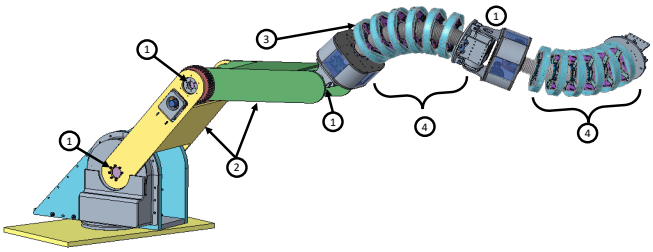

Fig. 1: ISCR concept drawing: ① revolute joints ② rigid links ③ sensor disk ④ continuum segment

To address these limitations, our ongoing research efforts focus on two aspects: 1) the creation of *in-situ collaborative robots* (ISCRs) to allow operators to guide these robots via physical interaction in confined spaces, 2) the exploration of intelligent robots with sensory awareness for *ex-situ* collaboration within semi structured environments. ISCRs will have to co-exist safely with a human operator in a confined space, therefore, the need for safety at the levels of sensing and actuation must be addressed. Such robots should be designed with minimal actuation torques needed to achieve the tasks to ensure passive safety measures (i.e. reduced risk to the operator even in the case of catastrophic control failure). Their sensing should allow them to predict collisions with unknown objects and humans and should ideally help the high-level controller use mapping capabilities for safeguarding against collision and to adjust pre-planned operations to match the actual geometry of the unstructured environment.

ISCRs designed to operate in deep confined spaces (e.g. airplane wings) have two conflicting demands: the long reach requires very strong actuators, which are contrary to user safety requirements. This conflict may be resolved in two ways: design of robots with intrinsic static-balancing capabilities [6] and/or endowing these robots with kinematic redundancy, sensing and control algorithms to allow bracing against the environment [7].

Using these task specifications, we are designing a new generation of ISCRs that can achieve safe bracing, mapping and physical human robot interaction. Figure 1 shows a concept of an ISCR with a statically-balanced articulated base robot and a combination of revolute joints and continuum segments. We chose the continuum robots [8] at the distal end of the robot since they are suited for navigating

† Corresponding author

[1]Department of Mechanical Engineering, Vanderbilt University, Nashville, TN 37235, USA (andrew.orekhov, garrison.l.johnston, c.abah, nabil.simaan)@vanderbilt.edu

[2]Robotics Institute at Carnegie Mellon University, Pittsburgh,PA 15213, USA (choset@cs.) cmu.edu

This work was supported by NSF awards #1734461 and #1734460 and by Vanderbilt and Carnegie Mellon internal university funds. A. Orekhov was supported by the NSF Graduate Research Fellowship under #DGE-1445197. C. Abah was partly supported by National Institutes of Health (NIH) award T32-EB02193 of the National Institute of Biomedical Imaging and Bioengineering.

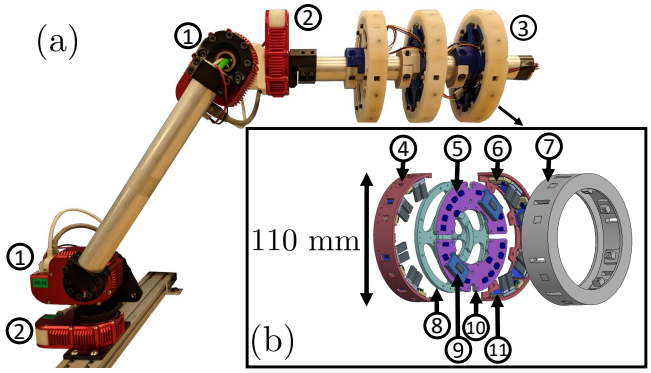

Fig. 2: (a) 4-DOF Robot: ① HEBI Robotics™ X8-16 actuator, ② HEBI Robotics™ X5-9 actuator, and ③ sensor disk units. (b) Exploded view of a sensing disk unit: ④ sensor mounting half-disk, ⑤ QWIIC I^{2}C connectors, ⑥ Hall-effect sensors, ⑦ silicone sleeve with embedded magnets, ⑧ core mounting disk, ⑨ multiplexer, ⑩ custom PCB, and ⑪ time-of-flight sensors.

confined spaces and their inherent compliance and low mass can further improve passive safety for physical human-robot interaction (pHRI).

To guarantee the safety of the operator, a host of technical challenges need to be addressed. One such challenge is providing additional sensing modalities to allow the robot to better anticipate and detect contact with the environment and with its operator. Most literature on contact detection with continuum robots focuses on applied wrench estimation using either measured loads on the actuation lines [9], measuring the deflection from an equilibrium position [10], using fiber Bragg gratings [11], or via kinematics based methods [12].

In [13], we proposed a sensor array for use in a continuum robot, where multiple sensing modalities are embedded within the spacer disks of the continuum robot. These sensor disks are being developed for eventual use in the continuum ISCR shown in Fig. 1. In addition to allowing for contact detection and localization, these sensor disks are equipped with time-of-flight (ToF) sensors to sense surrounding objects, anticipate contact with the robot, and map its environment.

In this paper, we discuss preliminary exploration of use of this sensor disk for pHRI. We describe a four degree-of-freedom robot with series-elastic joints and three sensor disks as shown in Fig. 2. We then give a description of the design of the sensor disk and provide four experimental proof-of-concept demonstrations of the potential use of the sensor disk for physical human-robot interaction.

II. Hardware Design and Fabrication

A. Robot Architecture

The experimental platform used in this paper is illustrated in Fig. 2. A 4 DOF serial robot was fabricated using four series elastic actuators as joints. The first and fourth joints were constructed using HEBI Robotics™ X5-9 actuators, and the other two joints used HEBI Robotics™ X8-16 actuators. The links of the robot include two aluminum hollow

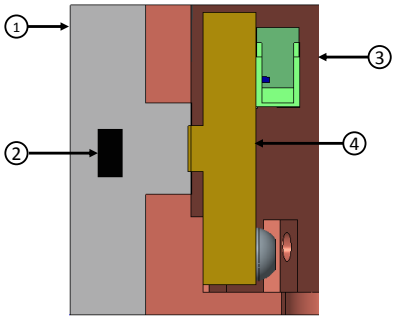

Fig. 3: Section view of the Hall-effect sensing components: a skin-like silicone rubber layer ① with embedded magnets ② is casted directly onto a half disk of the SDU ③, on which a Hall-effect sensor ④ is mounted.

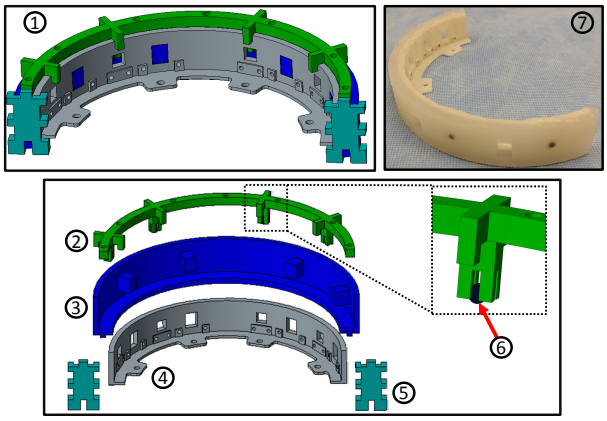

Fig. 4: ① Mold components assembled onto 3D-printed half-disk, ② custom fixture used to suspend the magnets at desired height and radial position, ③ mold with extrusions to maintain 9 mm $\times$7 mm windows for time-of-flight sensors, ④ half-disk on which the sensors are mounted, ⑤ side covers to clamp and seal the mold-disk assembly, ⑥ cylindrical magnet, and ⑦ prototype of silicone sleeve casted directly onto a 3D-printed SDU half disk.

tubes (length 12 in., diameter 1.25 in.) and two connecting brackets. Three sensing disk units (SDUs) are mounted on the distal link, with communication wiring passed through the tubes to the base of the robot. Although we show an embodiment with three disks, we note that in the experiments below, we used only the sensory information from a single distal sensing disk. The HEBI actuators are controlled using the HEBI MATLAB™ API, and the robot was powered with 24V.

B. Sensor Array Design

The SDU includes two main sensing modalities: a) time-of-flight sensing for mapping and proximity sensing, and b) Hall-effect sensing for contact detection and localization. An exploded view of a SDU is shown in Fig. 2b. Each disk consists of 8 time-of-flight sensors (VL6180X - ST Microelectronics) and 8 triaxis hall effect sensors (MLX90393, Melexis), mounted on the circumference of two 3D printed half-disks which have 9 mm $\times$ 7 mm windows to allow for

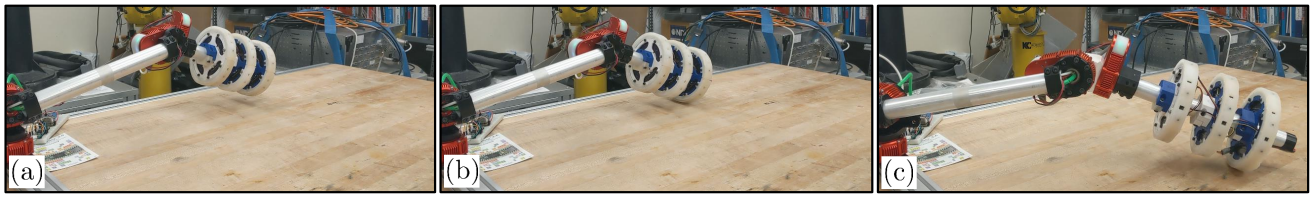

Fig. 5: The robot is shown (a) approaching the surface using its time-of-flight sensors, (b) making contact with surface, and (c) rolling along the surface.

ToF sensing. I^2C communication is used for data acquisition from all the sensors on all three disks. Multiplexers (two per disk) are used to by-pass the challenge of non-unique I^2C sensor addresses. Custom PCBs were designed to streamline the wiring within and between each sensor disk.

For the purpose of the proposed experiment, we aim to detect objects in close proximity to the robot, thus the VL6180X ToF sensors (range $0 - 100$ mm) were selected. Previous characterization experiments in [13] showed that the detection cone of these sensors ranges from $\pm 11.9°$ for glossy surfaces and $\pm 16.5°$ for matte surfaces.

Hall-effect sensing is implemented in each SDU for the purpose of contact detection and localization. As shown in Fig. 3, a 5 mm skin-like silicone rubber layer with embedded magnets was casted directly onto each half disk of the SDU. The embedded magnets were positioned to ensure radial alignment with the Hall-effect sensors. At rest, each magnet is 5 mm away from its corresponding hall effect sensor. When the sensor disk is subjected to an external load, the silicone deflects, resulting in motion of the magnets relative to the Hall-effect sensor. This motion is perceived as a change in the magnetic field detected by these sensors [14].

In addition to housing the magnets, the silicone also serves as a protection layer against harsh contact against the environment and humans. Thus, a shore 2A silicone elastomer (Dragon Skin Fx Pro, Reynolds Advanced Materials) was selected because it is soft enough to enable detectable displacement of the embedded magnets, yet hard enough to withstand contacts with the environment. Fig. 4 shows the mold used to cast the silicone skin directly onto the disk, and with embedded magnets. Silicone glue (Sil Poxy, Reynolds Advanced Materials) was used to reinforce the adhesion between the 3D printed disks and the silicone layer.

III. Experimental Results

In [13] we demonstrated feasibility of contact detection using the Hall-effect sensors and we showed the feasibility of actively mapping the environment using ToF sensors. In this experiment, we explored the feasibility of bracing using ToF sensors alone. If successful, this demonstrates that our design has fail-safe capabilities in case either one of the Hall-effect or ToF sensors fails. Since, in our previous work, we demonstrated mapping of the environment, we assumed some *a-priori* knowledge of the environment surface normal when defining the task of bracing.

We carried out four proof-of-concept demonstrations of the potential benefits of this manipulator architecture. The first shows a simple bracing experiment, which reduces the required actuator torques and can allow for collecting geometric data about the bracing surface. The second shows the robot avoiding contact with a human and the environment using its ToF sensors. The third demonstration shows a combination of the last two tasks of bracing while rolling on a surface and evading a user's hand. Finally, we show simple physical interaction with the robot using the Hall-effect sensors.

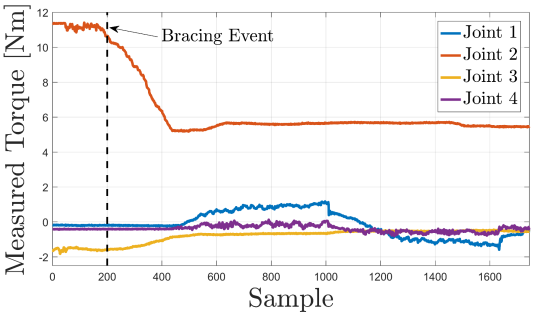

Fig. 6: Torques on the revolute actuators under a bracing point contact, which shows a reduction in the required torques for this trajectory.

A. Bracing Using ToF Sensors

In our first demonstration, the robot is mounted on a table and started at a predefined configuration roughly 200 mm above the table. The robot was then commanded to move downward with an end-effector speed as follows:

$$\|\boldsymbol{v}\| = \begin{cases} \frac{d_e}{d_{max}}(v_{max} - v_{min}) + v_{min} & d_e < d_{max} \\ v_{max} & d_e \geq d_{max} \end{cases} \quad (1)$$

where $\|\boldsymbol{v}\|$ is the norm of the velocity vector, d_e is the estimated distance to the surface, and d_{max} is the maximum distance that the sensor can detect. The distance d_e was determined using a moving average filter on the two ToF sensors that were oriented most normal to the table surface. Equation 1 reduces the velocity as the robot approaches the surface, allowing for a more precise bracing contact. We assumed contact was made with the surface once the moving average first returned a value below a minimal threshold of 1.5 mm. Once contact was detected in this way, we rolled the sensing disk back and forth along a circular arc on the surface of the table while recording the joint torque values.

We repeated this experiment, except the circular rolling motion was initiated when the estimated distance was 20 mm, causing the robot to roll in free space without bracing.

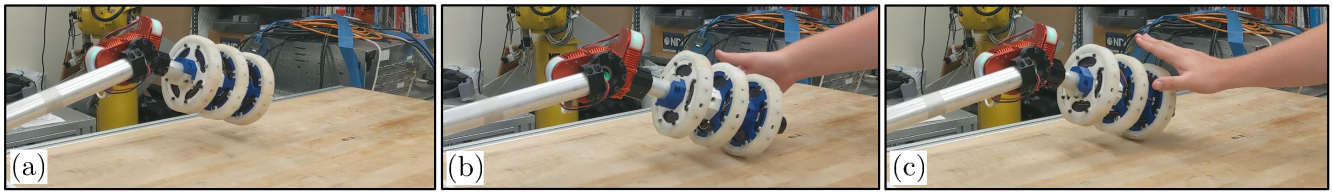

Fig. 7: The robot is shown (a) approaching the surface using its ToF sensors (and subsequently establishing a bracing contact), (b) rolling along the surface to avoid contact with a human, and (c) reversing direction of roll to avoid collision.

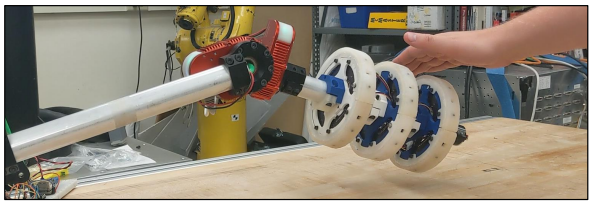

Fig. 8: Video snapshot of the robot using its time-of-flight sensors to avoid contact with both a human and the environment.

Figure 6 shows the joint torques when the robot was bracing. We note that just before Sample 500, the torques are significantly reduced due to the bracing contact. In free space, the joint torques stay roughly constant throughout the motion. Joint torques for this specific experiment were reduced by approximately 45% for Joint 2 (from 11 Nm to 6 Nm) and by approximately 70% for Joint 3 (from 1.6 Nm to 0.47 Nm). Joints 2 and 4 are roll joints that do not experience significant gravity loading in the direction of torque. We note that the compliance of the series elastic actuators allowed the manipulator to utilize bracing without us putting effort into calibrating the robot or environment model.

B. Interaction using Time-of-Flight Sensors

We also implemented a simple demonstration of how the manipulator might use the ToF sensors to avoid contact with the environment and/or a human worker. The measured ranges from the ToF sensors d_i were used to generate a set of velocity commands pointing towards the center of the disk and having a magnitude that increases with proximity to the center of the disk. These vectors are combined into a resultant end-effector velocity defined as the following:

$$\boldsymbol{v}_e = \alpha \sum_{i=1}^{8} \underbrace{\left(\frac{1+\text{sgn}(d_{max}-d_i)}{2}\right)}_{a_i} (d_i - d_{max})\ {}^0\mathbf{R}_{s_i}\ {}^{s_i}\hat{\mathbf{n}} \quad (2)$$

where α is a scalar gain to scale the resulting velocity vector, ${}^0\mathbf{R}_{s_i}$ is the rotation from i^{th} sensor frame to the world (frame $\{0\}$), sgn$(\cdot)$ is the sign function and ${}^{s_i}\hat{\mathbf{n}}$ is the outward-pointing radial vector normal to the i^{th} range sensor. The scalar a_i is 0 if $d_i > d_{max}$ and 1 otherwise.

The end-effector velocity vector $\boldsymbol{v}_e$ becomes the robot's task, and the joint velocities are given by:

$$\dot{\boldsymbol{q}} = \mathbf{J}^{+}\boldsymbol{v}_e \quad (3)$$

where $\mathbf{J}^{+}$ is the minimum-norm pseudo-inverse of the robot's translational Jacobian and $\dot{\boldsymbol{q}}$ are the joint velocities. We note that this particular implementation considered only a scenario of interacting with disks along the last link of the robot. Also, note that joint four did not affect the position of the end-effector and thus a normal inverse could have been used as well in this scenario.

Snapshots of a video showing a human interacting with the robot are provided in Fig. 5. The robot is moved in all directions using the ToF sensors, and at the end, the human guides the robot down towards the table, at which point the robot keeps an equal distance between the table and the human's hand.

C. Combined Interaction and Bracing using ToF Sensors

We also demonstrated combined bracing and collision avoidance using the ToF sensors. Video snapshots of this experiment are shown in Fig. 7. The robot starts in free space approximately 20 cm above the table, then establishes a bracing point using the same strategy described in Section III-A. Then, we use a scheme similar to what is described in Section III-B, except $\boldsymbol{v}_e$ is projected along a direction tangent to the circle on which the disks travels and in the plane of the assumed table surface. Rotation of the disk is coordinated with the velocity to avoid violating the no-slip rolling kinematic constraint between the disk and the table surface. We also ignore data from ToF sensors that point directly towards the table. Ignoring the data from these sensors helped to prevent unintended motion of the disk when no human contact was being detected, since in this simple interaction scheme, ToF sensors pointing directly at the surface can cause small motions to be induced due to different ToF sensor range values/sensor noise. As shown in Fig. 7, the robot is able to roll along the table surface while avoiding contact with a human.

D. Physical Interaction using Hall-effect Sensors

We also demonstrated simple physical interaction with the robot using the eight Hall-effect sensors on the distal sensor disk. In this demonstration, the time-of-flight sensors were not used, but as in Section III-B, the Hall-effect sensor data was used to generate a set of vectors pointing towards the center of the disk and having a magnitude directly proportional to the measured change in the magnetic field. These vectors were combined into a resultant end-effector velocity defined as:

$$\boldsymbol{v}_e = -\beta \sum_{i=1}^{8} |b_i - b_{avg,i}|\ {}^0\mathbf{R}_{s_i}\ {}^{s_i}\hat{\mathbf{n}} \quad (4)$$

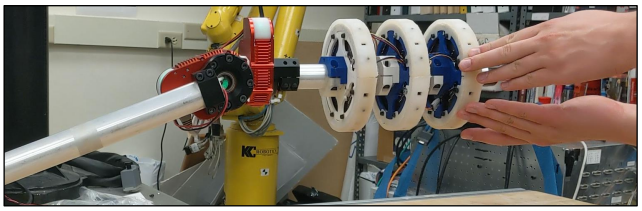

Fig. 9: Video snapshot of the robot using its Hall-effect sensors to respond to physical interaction from a user.

where β is a user-defined scalar gain, and for the ith Hall-effect sensor, b_i is the current sensor measurement and $b_{avg,i}$ is a 200-sample moving average of the sensor measurements. The moving average allows for changes in magnetic field to be detected without offline calibration. Similar to above, ${}^0\mathbf{R}_{s_i}$ is the rotation from the ith sensor frame to the world frame, and ${}^{s_i}\hat{\mathbf{n}}$ is the outward-pointing radial vector normal to the ith Hall-effect sensor.

The multimedia extension shows a user physically moving the robot in free space using several of the Hall-effect sensors. A snapshot of this video is shown in Fig. 9.

IV. Current Limitations

One limitation of our current system is limited speed of communication for the I^{2}C sensors. In all of the experiments presented, we have used only a single disk and are collecting data from the microcontroller via UDP communication to a MATLAB host. With this setup, we have been successfully acquiring time-of-flight proximity data at approximately 30 Hz, and Hall-effect sensor data at approximately 36 Hz. Initial tests with all three disks on a single I^{2}C bus have shown communication speeds dropping to roughly 18 Hz. We are currently investigating ways to improve the communication speed.

Another limitation is cross-talk between different time-of-flight sensors. In preliminary mapping experiments using all three sensing disks, we have observed an increase in noise due to interference between the sensors that seems to significantly degrade the accuracy of the mapping. Future work will investigate ways to mitigate these effects.

V. Conclusion

In this paper, we have presented an experimental platform for evaluating a multi-modal sensing disk unit that has potential applications in human-robot interaction for confined spaces. Experimental results showed the use of the disk for bracing against the environment and for collision avoidance using sensory data from the skin. Future work includes further integration of the sensing disk into a highly-redundant continuum manipulator and investigating redundancy resolution techniques that leverage these sensing modalities.

VI. Multimedia Extension

A video showing the experimental results of this paper can be viewed here: https://youtu.be/5X9QuTiORJk

References

[1] A. E. Barr and M. F. Barbe, "Pathophysiological tissue changes associated with repetitive movement: A review of the evidence," *Physical Therapy*, vol. 82, pp. 173–187, 2002.

[2] Occupational Safety and Health Administration. (2017) Prevention of work-related musculoskeletal disorders, [online]. https://www.osha.gov/pls/oshaweb/owadisp.show_document?p_table=UNIFIED_AGENDA&p_id=4481.

[3] G. Hirzinger, A. Albu-Schaffer, M. Hahnle, I. Schaefer, and N. Sporer, "On a new generation of torque controlled light-weight robots," pp. 3356–3363, 2001.

[4] M. Zinn, O. Khatib, B. Roth, and J. K. Salisbury, "Towards a human-centered intrinsically-safe robotic manipulator." *IEEE Robotics and Automation Magazine*, vol. 11, no. 2, pp. 12–21, 2004.

[5] A. De Santis, B. Siciliano, A. De Luca, and A. Bicchi, "An atlas of physical human-robot interaction," *Mechanism and Machine Theory*, vol. 43, no. 3, pp. 253–270, 2008.

[6] M. Vermeulen and M. Wisse, "Intrinsically Safe Robot Arm: Adjustable Static Balancing and Low Power Actuation," *International Journal of Social Robotics*, vol. 2, no. 3, pp. 275–288, 2010.

[7] D. Kondo, M. Itosima, M. Minami, and A. Yano, "Proposal of bracing controller utilizing constraint redundancy and optimization of bracing position," in *The SICE Annual Conference 2013*, Sep. 2013, pp. 2732–2737.

[8] G. Robinson and J. B. C. Davies, "Continuum robots - a state of the art," in *Proceedings 1999 IEEE International Conference on Robotics and Automation (Cat. No.99CH36288C)*, vol. 4, May 1999, pp. 2849–2854 vol.4.

[9] K. Xu, N. Simaan *et al.*, "An investigation of the intrinsic force sensing capabilities of continuum robots," *IEEE Transactions on Robotics*, vol. 24, no. 3, pp. 576–587, 2008.

[10] D. C. Rucker and R. J. Webster, "Deflection-based force sensing for continuum robots: A probabilistic approach," in *Intelligent Robots and Systems (IROS), 2011 IEEE/RSJ International Conference on*. IEEE, 2011, pp. 3764–3769.

[11] R. Xu, A. Yurkewich, and R. V. Patel, "Curvature, torsion, and force sensing in continuum robots using helically wrapped fbg sensors," *IEEE Robotics and Automation Letters*, vol. 1, no. 2, pp. 1052–1059, 2016.

[12] A. Bajo and N. Simaan, "Kinematics-based detection and localization of contacts along multisegment continuum robots," *IEEE Transactions on Robotics*, vol. 28, no. 2, pp. 291–302, 2012.

[13] C. Abah, A. Orekhov, G. Johnston, Y. Peng, H. Choset, and N. Simaan, "A multi-modal sensor array for safe human-robot interaction and mapping," in *2019 IEEE International Conference on Robotics and Automation (ICRA)*. IEEE, 2019.

[14] T. Paulino, P. Ribeiro, M. Neto, S. Cardoso, A. Schmitz, J. Santos-Victor, A. Bernardino, and L. Jamone, "Low-cost 3-axis soft tactile sensors for the human-friendly robot vizzy," in *Robotics and Automation (ICRA), 2017 IEEE International Conference on*. IEEE, 2017, pp. 966–971.